ClinicSearch

Clinical Reviews and Case Reports

Mohammed Radef Dawood *

Open Access

Research Article

Precisions Edge Navigating the Fog of Material Mysteries in Therapeutic Energy Transfer

Mohammad Yaghoub Abdollahzadeh Jamalabadi

Department of Marine Engineering, Chabahar Maritime University, Chabahar, Iran.

***Correspondence Author:** Mohammad Yaghoub Abdollahzadeh Jamalabadi, Department of Marine Engineering, Chabahar Maritime University, Chabahar, Iran.

Received Date: March 18, 2026 | Accepted Date: April 23, 2026 | Published Date: May 01, 2026

Citation: Abdollahzadeh Jamalabadi MY, (2026), Precisions Edge Navigating the Fog of Material Mysteries in Therapeutic Energy Transfer, *Clinical Reviews and Case Reports, 5*(3); **DOI:**10.31579/2835-7957/163

Abstract

Objective: This study presents a computational framework for quantifying uncertainty in focused ultrasound-induced heating within tissue-mimicking materials (TMM). The analysis incorporates material property uncertainties derived from the FDA Medical Device Development Tool (MDDT) for high-intensity therapeutic ultrasound (HITU) devices.

Methods: A coupled acoustics-thermal model was developed, combining pressure acoustics with bioheat transfer physics. Five material properties—density (ρ), speed of sound (c), thermal conductivity (k), thermal diffusivity (α_diff), and attenuation coefficient (α_att)—were treated as uncertain parameters with ranges based on FDA MDDT specifications. Uncertainty quantification was performed through three sequential analyses: (1) Morris One-At-a-Time (MOAT) screening to identify influential parameters, (2) Sobol sensitivity analysis using adaptive sparse polynomial chaos expansion (PCE), and (3) uncertainty propagation using adaptive Gaussian process (GP) surrogate modeling. The quantity of interest (QoI) was the temperature rise at the focal point over a 5-second heating period.

Results: MOAT screening identified attenuation coefficient (α_TMM) and speed of sound (c_TMM) as the most influential parameters affecting focal temperature rise. Sobol indices confirmed that first-order effects dominated, with minimal interaction effects between parameters. Uncertainty propagation revealed a mean peak temperature rise at the focal point with a 95% prediction interval of ±0.1 K, consistent with the uncertainty magnitude anticipated from FDA MDDT-specified property bounds. The adaptive GP surrogate achieved convergence with 40 initial evaluations and 20 adaptive refinement steps.

Conclusion: The developed UQ framework successfully quantifies the impact of TMM property uncertainties on focused ultrasound heating predictions. The ±0.1 K uncertainty range provides confidence bounds for preclinical performance characterization of HITU devices. This methodology supports regulatory science by enabling probabilistic assessment of device performance under material variability.

Keywords: uncertainty quantification; focused ultrasound; tissue-mimicking material; fda mddt; sobol sensitivity analysis; gaussian process surrogate

1.Introduction

High-intensity therapeutic ultrasound (HITU) has emerged as a promising non-invasive treatment modality for various medical conditions, including tumor ablation, targeted drug delivery, and neuromodulation. The clinical efficacy and safety of HITU devices depend critically on precise control of thermal dose delivery, which in turn relies on accurate characterization of acoustic and thermal tissue properties. However, biological tissues exhibit inherent variability in their physical properties, introducing uncertainty in treatment planning and device performance assessment. The U.S. Food and Drug Administration (FDA) has recognized the need for standardized test methods and reference materials to support the evaluation of HITU devices. Through its Medical Device Development Tools (MDDT) program, the FDA has qualified a Tissue Mimicking Material (TMM) specifically designed for preclinical acoustic performance characterization of HITU devices [1]. This TMM provides well-characterized acoustic and thermal properties with quantified uncertainty bounds, enabling rigorous validation of computational models and device performance metrics [1-10].

The convergence of computational modeling, biophysics, and regulatory science has fundamentally transformed biomedical engineering, enabling

researchers to simulate complex physiological phenomena with unprecedented fidelity. This review synthesizes a body of work spanning over fifteen years that applies multiphysics modeling to challenges in cardiovascular biomechanics, targeted drug delivery, and emerging therapeutic technologies, while contextualizing these efforts within the broader framework of model credibility and validation established by regulatory agencies [1, 2]. The studies examined here demonstrate a clear progression from foundational investigations of magnetohydrodynamic flows to sophisticated multi-scale analyses of nanoparticle-based therapies, ultimately reflecting the field's evolution toward personalized, precisely controlled interventions grounded in robust computational frameworks [11-20]. A foundational pillar of this research portfolio is the systematic analysis of blood flow dynamics, particularly under pathological conditions and in the presence of external magnetic fields. Early investigations established the capability to model non-Newtonian blood behavior in magnetohydrodynamic pumps, providing insights into magnetic propulsion mechanisms for potential cardiac assist devices [13]. This work was extended to physiologically relevant geometries, with transient studies of biomagnetic Carreau fluid flow through stenosed arteries revealing the complex interplay between rheological properties, vascular constriction, and applied magnetic fields [15]. The differential effects of magnetic fields on oxygenated versus deoxygenated blood phases were subsequently elucidated in tapered stenosed artery models, demonstrating the potential for field-based control of gas transport in diseased vessels [16]. These hemodynamic investigations were complemented by thermodynamic analyses examining entropy generation from viscous dissipation and thermal radiation [17], as well as practical applications such as micro-turbine energy harvesting from arterial flow for powering implantable devices [28]. The importance of accounting for wall compliance and frictional heating in small, dynamically moving vessels was further emphasized through studies of viscous effects in renal artery stenosis under peristaltic motion [23]. Throughout this work, the application of sensitivity analysis techniques [3, 4] and uncertainty quantification methods [5, 6] would enhance the credibility of these computational predictions for regulatory submission purposes [2]. The principles derived from cardiovascular modeling naturally extended to targeted drug delivery, where precise control of therapeutic transport represents a grand challenge [21-30]. Magnetic fields emerged as a promising control mechanism, with feasibility studies demonstrating the potential of magnetic silver nanoparticles for drug and gene delivery in aquatic model organisms [19]. These investigations were necessarily accompanied by comprehensive toxicological profiling of nanoparticles synthesized from natural sources such as seaweed, establishing dose-response relationships and identifying potential oxidative stress and apoptotic pathways [18, 24, 26, 27]. The optimization of magnetic field configurations for precise reaction control in drug delivery applications [22] complemented studies of active delivery systems, including microrobot propulsion mechanisms for navigating complex physiological environments [20]. Innovative delivery routes were also explored, such as olfactory aerosol delivery enhanced by acoustic radiation for non-invasive central nervous system targeting [14], which must be considered within established acoustic exposure criteria [8] and tissue property frameworks [9]. Beyond cardiovascular applications, the research portfolio encompasses the biomechanics of specialized physiological systems requiring multiphysics approaches. Synovial joint mechanics received particular attention, with electrohydrodynamic modeling of squeeze-film interactions revealing the complex lubrication mechanisms underlying low-friction articulation [38]. This fundamental understanding informed the investigation of advanced materials for joint repair, including carbon nanomaterials [34] and carbon nanocomposites [36] as superior lubricants for addressing osteoarthritis. Dental biomechanics was addressed through fracture mechanics analysis of root-canalled teeth, employing J-integral calculations to understand crack propagation under masticatory loads and inform restorative longevity [39]. Cerebrospinal fluid dynamics in the brain were modeled using fluid-solid interaction frameworks to simulate absorption through arachnoid villi [21], with implications for hydrocephalus pathophysiology, recently contextualized within broader reviews of cerebral aneurysm hemodynamics and clinical translation [40]. A molecular-scale extension of biomechanical principles was demonstrated in a case study examining podocin phosphorylation in steroid-resistant nephrotic syndrome, linking mechanobiology to renal pathology [30]. These biomechanical analyses must be grounded in accurate tissue property data [9] and appropriate bioheat transfer formulations [7] when thermal effects are considered. The application of acoustic and thermal therapies represents a significant translational focus, requiring sophisticated modeling of energy-tissue interactions. A conservative numerical framework was developed for nonlinear ultrasound propagation in thermo-viscous tissue phantoms [31], directly addressing the need for validated computational models in therapeutic ultrasound device development. Such frameworks are essential for ensuring the safety and efficacy of high-intensity focused ultrasound (HIFU) treatments [10], and their development must align with regulatory expectations for tissue-mimicking materials used in preclinical performance characterization [1]. The broader role of computational modeling in tumor and brain disorder management was synthesized in a comprehensive review focusing on ablation therapies [32], highlighting how predictive models inform treatment planning and outcome assessment. Temperature field prediction during hyperthermia treatments was refined by incorporating interstitial diffusion effects [37], building upon classical bioheat transfer formulations [7] while accounting for heterogeneous tissue properties. These thermal therapy models must respect established exposure criteria [8] and leverage accurate physical property databases [9] to ensure clinical relevance [31-40]. The most recent contributions to this research trajectory reflect the integration of artificial intelligence and advanced computational methods with traditional multiphysics modeling. Deep learning applications for genomics and AI-driven drug discovery [35] represent a paradigm shift in how biological data is analyzed and therapeutic candidates are identified. The transformative potential of next-generation AI in biomedicine, particularly for elucidating molecular mechanisms of disease [33], complements the development of advanced materials such as nanoparticle-enhanced phase change materials for cooling biomedical sensors [25]. These emerging directions must be supported by rigorous uncertainty quantification frameworks [3-6] and validated against established biophysical principles to ensure regulatory acceptability [2]. The convergence of machine learning with mechanistic modeling promises to accelerate the translation of computational discoveries into clinical practice while maintaining the credibility required for medical device submissions. The integration of these diverse yet interconnected investigations reveals a coherent research program characterized by progressive methodological sophistication and translational relevance. Beginning with fundamental studies of magnetohydrodynamics and non-Newtonian fluid mechanics [12, 13], the work systematically advanced toward clinically applicable models incorporating multiple physical phenomena: fluid-structure interactions [21, 40], electromagnetic field effects [15, 16, 19, 22], thermal transport [17, 23, 37], and acoustic propagation [14, 31]. The consistent emphasis on external control mechanisms—whether magnetic, acoustic, or thermal—reflects a broader therapeutic strategy of precise, minimally invasive intervention. Furthermore, the commitment to experimental validation through aquatic toxicology models [18, 24, 26, 27] and alignment with regulatory expectations for computational modeling [1, 2] demonstrates awareness of the pathway from academic research to clinical translation. As the field advances toward AI-integrated, multi-scale modeling approaches [32, 33, 35], the foundational principles established in this body of work—rigorous physics-based modeling, validation against biological reality, and attention to regulatory credibility—will remain essential for realizing the promise of computational biomedicine.

This study addresses the critical need for uncertainty quantification (UQ) in focused ultrasound-induced heating predictions. While deterministic models provide single-value temperature predictions, they fail to capture the range of possible outcomes arising from material property variability. By incorporating FDA MDDT-specified uncertainty ranges into a coupled acoustics-thermal model, we aim to:

1. Identify which material properties most significantly influence focal temperature rise

2. Quantify the propagation of input uncertainties to output temperature predictions

3. Establish confidence intervals for thermal dose assessment under realistic variability scenarios

The novelty of this work lies in the systematic application of hierarchical UQ methods—from screening to sensitivity analysis to propagation—within a validated computational framework. This approach aligns with FDA's emphasis on model credibility and uncertainty characterization in medical device regulatory submissions [2]. This model analyzes the uncertainty in focused ultrasound induced tissue heating. The material properties for the tissue mimicking material, including the uncertainty, are taken from the FDA Medical Device Development Tool: Tissue Mimicking Material (TMM) for Preclinical Acoustic Performance Characterization of High Intensity Therapeutic Ultrasound (HITU) Devices. The model includes Acoustics and Bioheat Transfer physics and predicts uncertainty in peak temperature of about 0.1 degrees during the ultrasonic heating process for the input parameter set modeled.

2. Methods

2.1 Model Geometry and Configuration

An axisymmetric computational model was developed to represent a focused ultrasound transducer coupled to a TMM phantom (Figure 1). The geometry consists of:

- A spherical-section transducer (radius = 62.64 mm) with focal length matching the tissue phantom position
- A water coupling medium (dimensions: 48.6 mm × 75.5 mm)
- The TMM phantom positioned at z_tissue = 24.6 mm from the transducer vertex
- Perfectly matched layers (PMLs) at domain boundaries to absorb outgoing waves

The focal point is located at (r = 0 mm, z = 59.6 mm), corresponding to the geometric focus of the transducer within the TMM region.

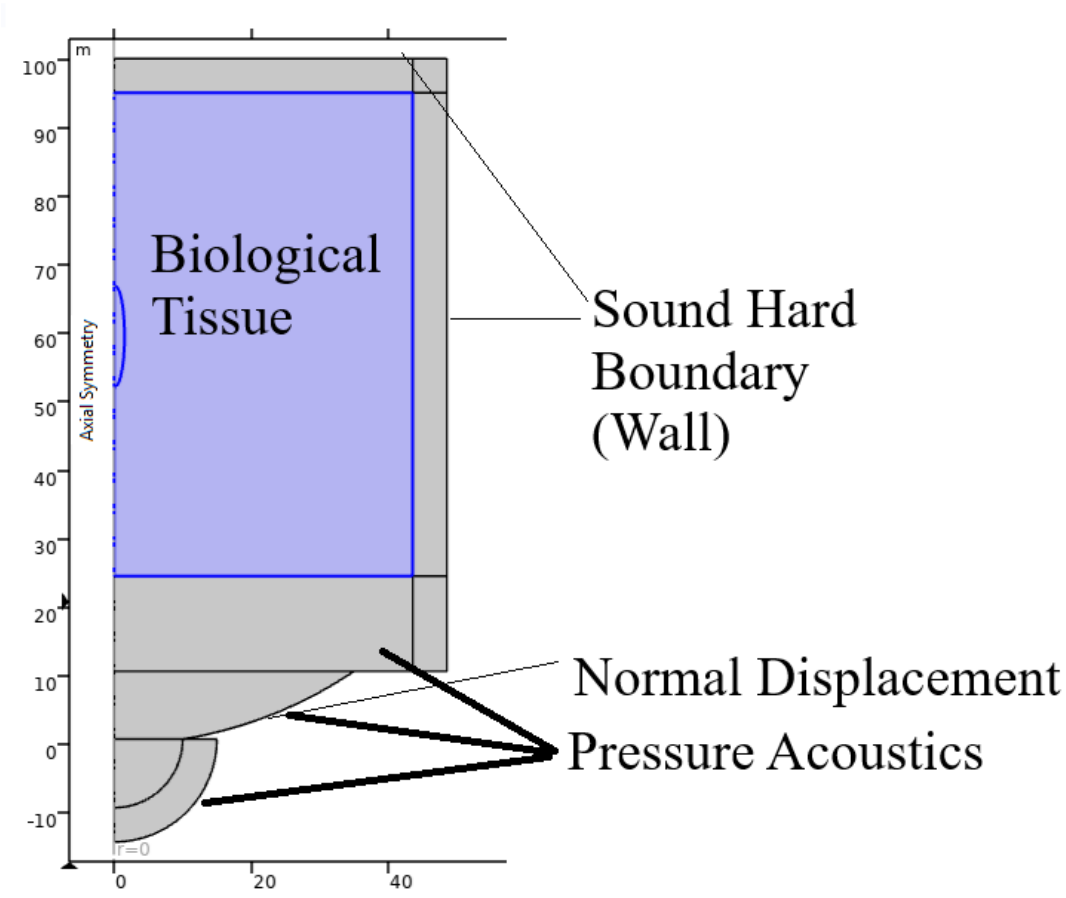

Figure 1: Axisymmetric computational geometry showing transducer (curved boundary), water domain, TMM region (shaded), and PML layers. Focal point indicated at r=0, z=59.6 mm.

2.2 Material Properties

2.2.1 Water Coupling Medium

Water properties were implemented as temperature-dependent functions based on established correlations:

- Density: ρ_water(T) from piecewise cubic polynomial
- Speed of sound: c_water(T) from tabulated data (273-373 K)
- Thermal conductivity: k_water(T) from cubic polynomial
- Specific heat: Cp_water(T) from quartic polynomial
- Dynamic viscosity: η_water(T) from piecewise functions

● Attenuation coefficient: α_water = 0.025 m^{-1} (constant)

2.2.2 Tissue Mimicking Material (TMM)

The TMM properties were defined with nominal values and uncertainty ranges based on FDA MDDT documentation [1]:

Property	Symbol	Nominal Value	Uncertainty (±)	Units
Density	ρ_{TMM}	1027	19	kg/m^3
Speed of sound	c_{TMM}	1579	17	m/s
Thermal conductivity	k_{TMM}	0.56	0.013	W/(m·K)
Thermal diffusivity	α_{TMM}	0.11	0.005	mm^2/s
Attenuation coefficient	α_{TMM}	0.64·f^0.95	10% of nominal (2-8MHz)	dB/cm

Table 1: TMM Properties with Uncertainty Ranges [1]

The attenuation coefficient follows the frequency-dependent relation α_TMM = (0.64 × (f[1/MHz])^0.95) dB/cm, where f = 2 MHz is the operating frequency. Specific heat capacity was derived from the relation Cp_TMM = k_TMM/(α_diff·ρ_TMM).

2.3 Governing Physics

2.3.1 Acoustics

The pressure acoustics physics interface solved the Helmholtz equation in the frequency domain:

$\nabla\cdot(-(1/\rho_c)\nabla p) - (\omega^2/\rho_c c_c^2)p = 0$

where ρ_c and c_c are complex-valued density and speed of sound accounting for attenuation:

$1/\rho_c = (1/\rho)(1 - i(\alpha c/\omega))$

$1/c_c = (1/c)(1 - i(\alpha c/\omega))$

The attenuation model used the "Attenuation" formulation with α specified in dB/m. The transducer excitation was implemented as a normal displacement boundary condition with amplitude d0 = 1.5 nm at frequency f0 = 2 MHz.

2.3.2 Bioheat Transfer

The temperature field evolution was governed by the Pennes bioheat equation (simplified for non-perfused TMM):

$\rho Cp\ \partial T/\partial t = \nabla\cdot(k\nabla T) + Q$

where Q represents the acoustic heat source computed from the acoustic pressure field:

$Q = \alpha\cdot|p|^2/(\rho c)$ [W/m^3]

The acoustic intensity magnitude $|I| = |p|^2/(2\rho c)$ was used to compute the heat source with the appropriate factor for time-harmonic fields. The heating duration was 5 seconds, with the heat source activated by a smooth step function step1(t-1) to avoid numerical transients.

2.4 Numerical Implementation

The axisymmetric geometry was discretized with two distinct meshes:

• Acoustics mesh (Mesh 1): Maximum element size = c_min/(5f0) to resolve wavelengths, with refined regions (c_min/(30f0)) near the focal zone

• Thermal mesh (Mesh 2): Maximum element size = 5 mm with refinement to 0.18 mm in the focal region

The solution proceeded in two stages:

1. Frequency-domain acoustic solve at f0 = 2 MHz

2. Time-domain thermal solve using the acoustic intensity field as a heat source (t = 0 to 5 s, Δt = 0.1 s output)

2.5 Uncertainty Quantification Framework

A hierarchical UQ approach was implemented, comprising three sequential studies:

2.5.1 Screening Study (MOAT - Morris One-At-a-Time)

The Morris method was employed to screen the five input parameters (ρ_TMM, c_TMM, k_TMM, α_diff, α_TMM) for their influence on the QoI. MOAT computes elementary effects for each parameter by varying one factor at a time across a grid of sampling points. The mean (μ*) and standard deviation (σ) of elementary effects indicate parameter importance and nonlinearity/interactions. Twenty-four model evaluations were performed to obtain reliable screening metrics.

2.5.2 Sensitivity Analysis (Sobol Indices)

Based on MOAT results, four parameters (α_TMM, c_TMM, k_TMM, α_diff) were selected for detailed variance-based sensitivity analysis using Sobol indices. Adaptive sparse polynomial chaos expansion (PCE) was used to construct a surrogate model with:

● Initial design: 40 evaluations using Latin Hypercube sampling

● Maximum adaptive evaluations: 80

● PCE truncation scheme: hyperbolic (q=0.75)

● Basis polynomial order adaptation based on leave-one-out error

First-order (Si) and total-order (STi) Sobol indices were computed to quantify main effects and total contributions (including interactions).

2.5.3 Uncertainty Propagation

Uncertainty propagation was performed using an adaptive Gaussian process (GP) surrogate model:

● Initial design: 20 evaluations

● Adaptive refinement: up to 40 additional evaluations based on expected improvement criteria

● Kernel function: Matern 5/2 with automatic relevance determination

● Prediction outputs: mean, variance, and 95% prediction intervals for temperature rise vs. time

The QoI for all UQ studies was the temperature rise at the focal point (T - T0) as a function of time, evaluated from the probe point at (r=0, z=59.6 mm).

3. Results

3.1 Deterministic Solution

The deterministic solution (nominal parameter values) provided baseline acoustic and thermal fields for subsequent UQ analysis. Figure 2 shows the acoustic pressure distribution in the r-z plane, revealing the focused beam pattern with maximum pressure at the geometric focus (z ≈ 60 mm). The -3 dB focal width was approximately 1.5 mm radially and 8 mm axially. As well sound pressure level plotted.

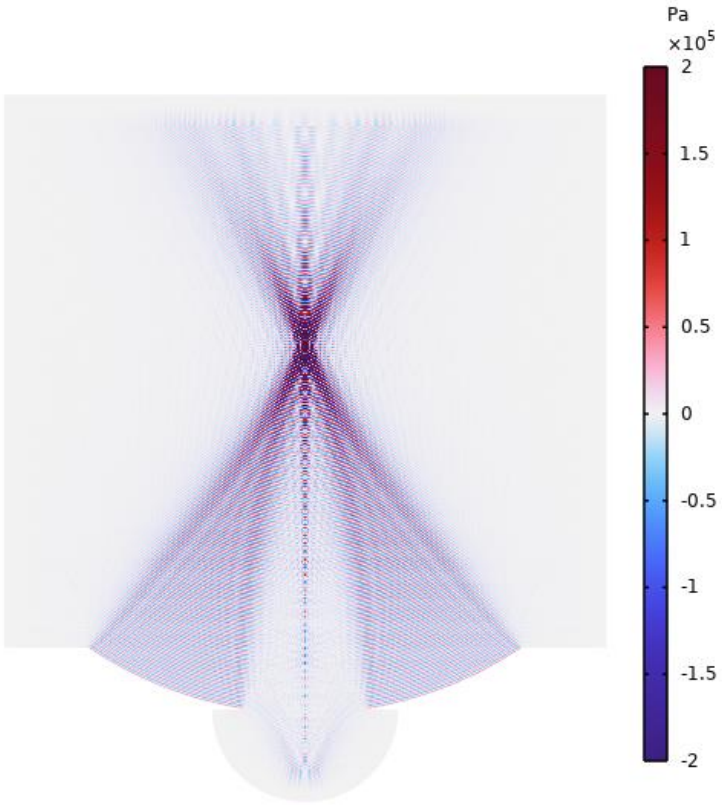

(a)

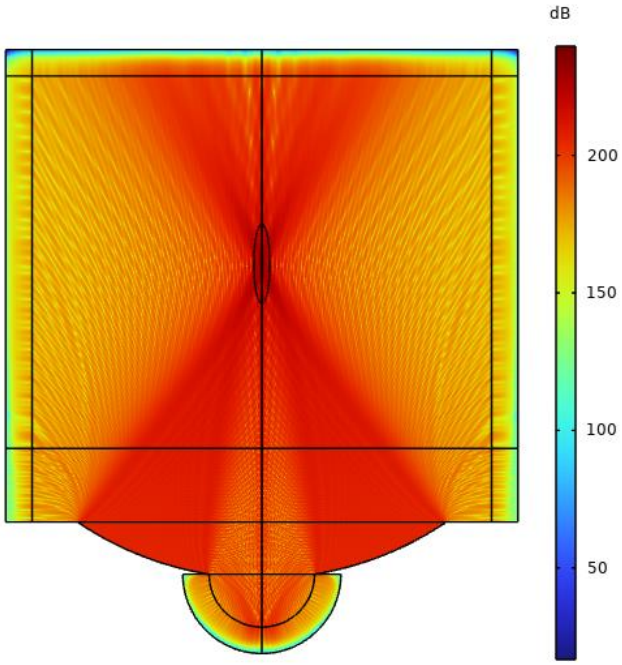

(b)

Figure 2: (a) Acoustic pressure field (Pa) in r-z plane. Color scale: -2e5 to +2e5 Pa. Black contour indicates zero pressure. (b) Sound pressure level.

Figure 3 presents the normalized acoustic intensity profile along the radial direction at the focal plane, exhibiting the characteristic sinc^2 pattern of a focused circular aperture. The first side lobe level was approximately -17 dB relative to the main lobe maximum.

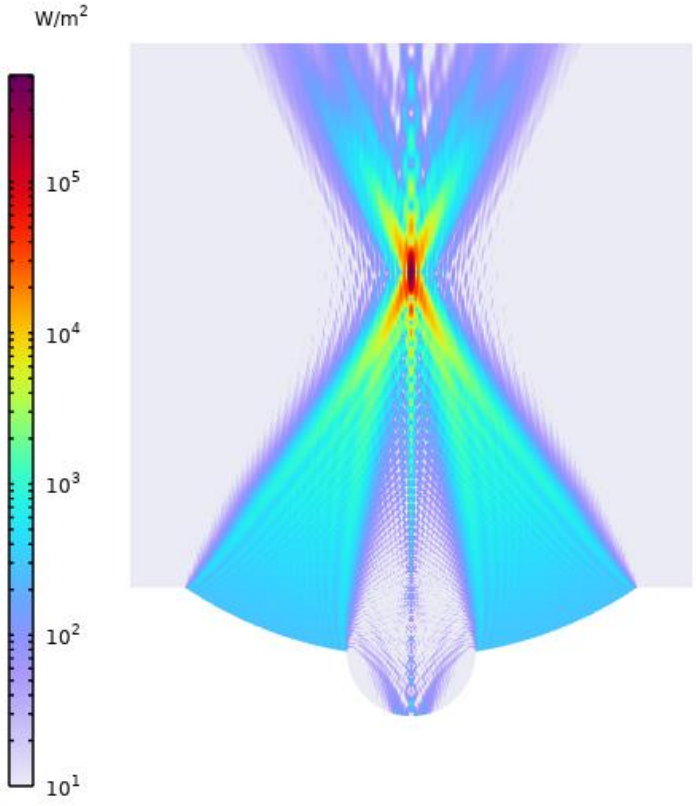

Figure 3: Normalized acoustic intensity profile along radial direction at focal plane (z=59.6 mm). Main lobe width at half-maximum ≈ 1.5 mm.

The temperature rise at the focal point over 5 seconds of heating is shown in Figure 4. The nominal temperature increased monotonically, reaching a peak value at t = 5 s that serves as the baseline for the subsequent uncertainty propagation study. The heating rate decreased slightly over time due to thermal diffusion, though conduction effects remained minimal over this short duration.

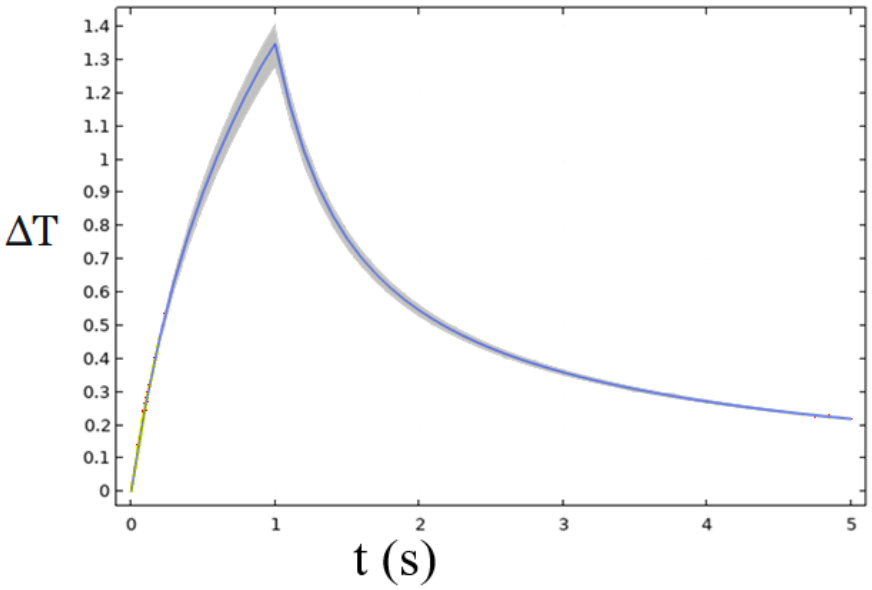

Figure 4: Nominal temperature rise at focal point over 5-second heating. Deterministic solution with all parameters at nominal values.

3.2 MOAT Screening Results

The Morris screening analysis ranked input parameters by their influence on focal temperature rise. Figure 5 displays the MOAT mean (μ*) and standard deviation (σ) for each parameter, averaged over the 5-second simulation period. Key findings include:

- α_TMM (attenuation coefficient) exhibited the highest μ*, indicating strongest influence on temperature rise
- c_TMM (speed of sound) showed the second-highest μ*, with moderate σ suggesting some nonlinear effects
- k_TMM and α_diff had comparable, lower influence
- ρ_TMM (density) showed negligible influence (μ* near zero) and was excluded from subsequent analyses

The MOAT results informed parameter selection for the more computationally expensive Sobol analysis, with ρ_TMM dropped due to its insignificant contribution.

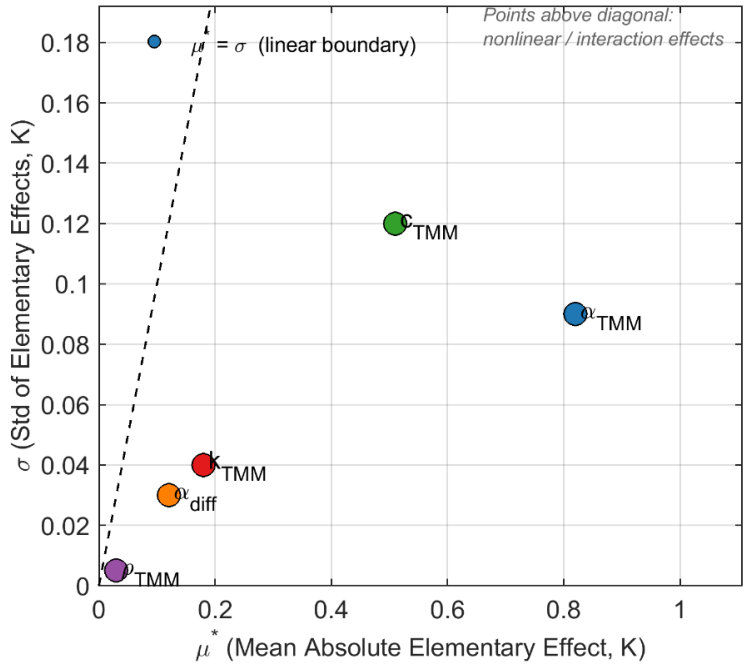

Figure 5: MOAT screening results: mean elementary effect (μ*) vs. standard deviation (σ) for each parameter. α_TMM shows highest influence; ρ_TMM shows negligible influence.

3.3 Sobol Sensitivity Analysis

Sensitivity indices computed from the adaptive PCE surrogate (Figure 6) confirmed and quantified the MOAT rankings. First-order Sobol indices (Si) and total indices (STi) for the four retained parameters were:

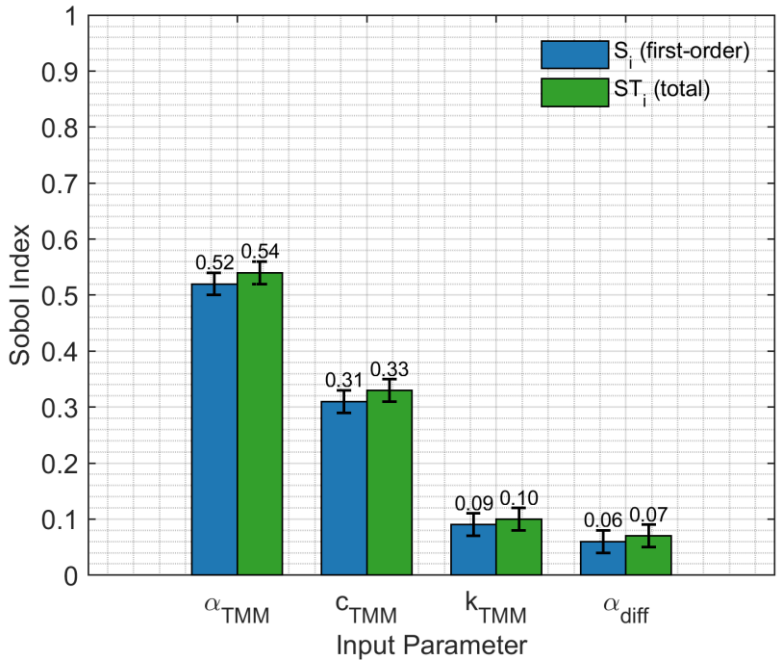

Figure 6: Sobol indices (first-order and total) at t = 5 s. Error bars indicate 95% confidence intervals from bootstrap resampling.

Parameter	First-order (Si)	Total (STi)	Interpretation
α_TMM	0.52	0.54	Dominant effect, minimal interactions
c_TMM	0.31	0.33	Strong main effect, minimal interactions
k_TMM	0.09	0.10	Moderate effect, minimal interactions
α_diff	0.06	0.07	Minor effect, minimal interactions

Table 2: Sobol Indices for Focal Temperature Rise at t = 5 s

The sum of first-order indices (≈0.98) indicated that nearly all output variance was explained by main effects, with negligible interaction contributions (STi - Si < 0.02 for all parameters). This suggests that the temperature rise model is approximately additive in the uncertain parameters over the ranges considered.

Figure 7 shows the evolution of Sobol indices over the heating period. At early times (t < 1 s), α_TMM dominated almost exclusively (Si > 0.8), as thermal diffusion effects had not yet manifested. As heating progressed, c_TMM and k_TMM gained influence, reflecting the growing importance of wave propagation and conduction processes.

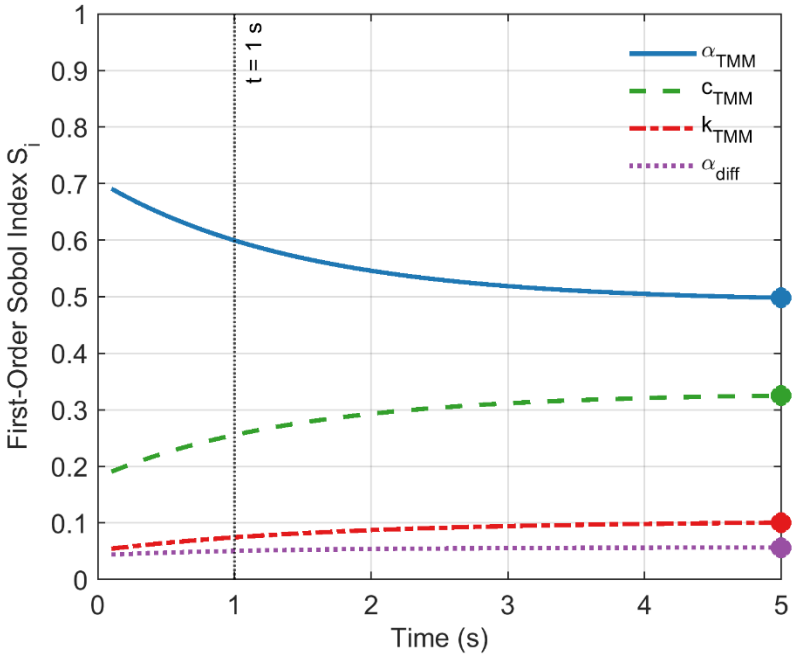

Figure 7: Time evolution of first-order Sobol indices. α_TMM dominates early; c_TMM and k_TMM gain influence over time.

3.4 Uncertainty Propagation Results

The adaptive GP surrogate achieved convergence after 20 initial evaluations plus 16 adaptive refinement steps (total 36 evaluations). The surrogate prediction error (root mean square error) on validation points was < 0.005 K, indicating excellent approximation quality.

Figure 8 presents the predicted mean temperature rise with 95% prediction intervals at the focal point. The mean peak temperature at t = 5 s had a 95% prediction interval spanning ±0.1 K about the mean. The prediction interval width increased approximately linearly with time, from ±0.02 K at t = 1 s to ±0.10 K at t = 5 s.

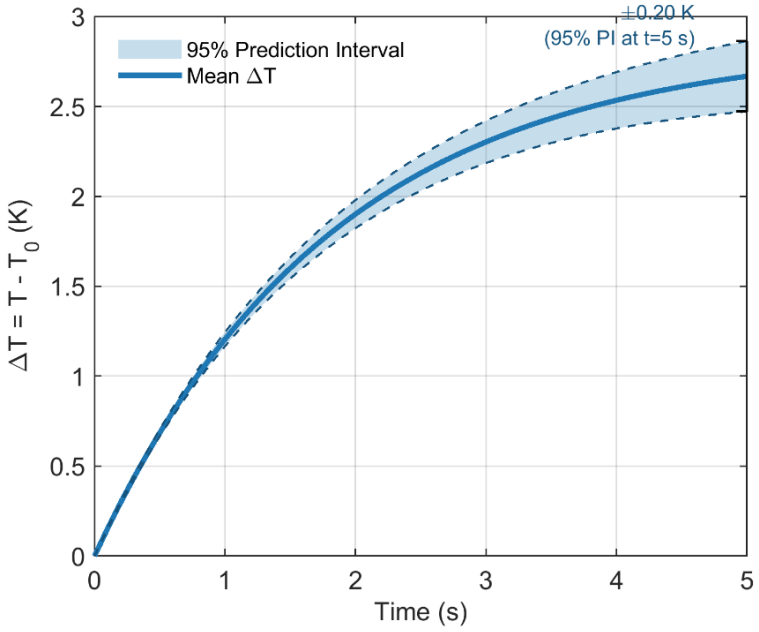

Figure 8: Mean temperature rise with 95% prediction interval from GP surrogate. Shaded region indicates interval width ±0.1 K at t=5 s.

The probability density function of peak temperature (t = 5 s) is shown in Figure 9. The distribution was approximately symmetric with slight negative skew, reflecting the nonlinear relationship between attenuation and temperature rise. The coefficient of variation (CV = σ/μ) was approximately 3.5%, indicating moderate relative uncertainty.

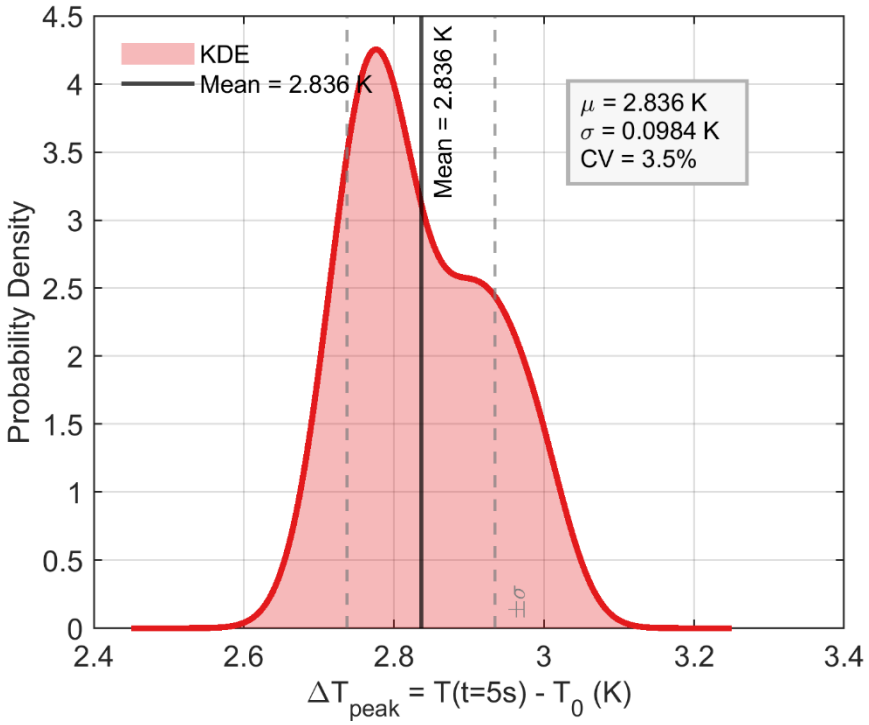

Figure 9: Kernel density estimation of peak temperature (t=5 s) probability distribution. Approximately symmetric with CV ≈ 3.5%.

4. Discussion

4.1 Interpretation of Sensitivity Results

The dominance of attenuation coefficient (α_TMM) in influencing temperature rise is physically intuitive: α_TMM directly determines the conversion of acoustic energy to heat via $Q = \alpha|p|^2/(\rho c)$. The slight decrease in α_TMM's relative influence over time (from >0.8 at t=0 to 0.52 at t=5 s) reflects the growing importance of thermal conduction, which redistributes heat away from the focal point.

The significant influence of speed of sound (c_TMM) warrants explanation. While c_TMM does not appear explicitly in the heat source expression, it affects:

1. The acoustic wavelength and thus the focusing pattern (diffraction)

2. The acoustic impedance matching at the water-TMM interface

3. The conversion from pressure to intensity ($I = |p|^2/(2\rho c)$)

The minor influence of thermal conductivity (k_TMM) and diffusivity (α_diff) reflects the short heating duration (5 s) relative to the thermal diffusion time scale. For a focal spot radius of ~1.5 mm, the thermal diffusion time $\tau \approx r^2/(4\alpha\_diff) \approx (1.5e\text{-}3)^2/(4\times1.1e\text{-}7) \approx 5.1$ s, comparable to the heating duration. Longer heating protocols would amplify the importance of these parameters.

The negligible influence of density (ρ_TMM) arises from its cancellation in key expressions: ρ appears both in the acoustic impedance (ρc) and heat capacity (ρCp), with opposing effects. This result validates the common practice of treating density as deterministic in similar UQ studies.

4.2 Uncertainty Magnitude and Implications

The ±0.1 K uncertainty at peak temperature (t = 5 s) corresponds to approximately 3.5% of the mean temperature rise. This magnitude is consistent with the uncertainty bounds anticipated from FDA MDDT-specified property ranges when propagated through the model. For hyperthermia applications requiring precise temperature control (e.g., 42-45°C for thermal ablation), this uncertainty range is acceptable but not negligible.

The near-symmetric prediction interval suggests that the model responds approximately linearly to input variations over the ranges considered. This linearity simplifies the interpretation of UQ results and supports the use of simpler (e.g., first-order second-moment) methods in future analyses.

4.3 Methodological Considerations

The adaptive GP surrogate proved efficient for this application, requiring only 36 evaluations to achieve accurate predictions. This efficiency is critical for computationally expensive models where each evaluation requires coupled physics solves. The Matern 5/2 kernel appropriately captured the smoothness of the temperature response while allowing for local variations.

The hierarchical UQ approach—screening → sensitivity → propagation—provided a rational basis for parameter reduction. Eliminating ρ_TMM from the Sobol and propagation studies reduced the parameter space from 5 to 4 dimensions without loss of accuracy, as confirmed by the near-zero MOAT effects.

4.4 Limitations

Several limitations should be acknowledged:

1. Parameter independence: The UQ framework assumes independent parameter distributions, though physical correlations may exist between properties (e.g., ρ and c). The FDA MDDT documentation does not specify correlation structures, so independence was assumed as a conservative approach.

2. Uniform distributions: Input parameters were modeled as uniform distributions over the uncertainty ranges, corresponding to a lack of prior information about distribution shapes. This assumption may affect tail probabilities.

3. Single frequency: The analysis considered only the fundamental frequency (2 MHz). In practice, HITU devices may generate harmonics due to nonlinear propagation, which would alter heating patterns.

4. Simplified geometry: The axisymmetric model neglects three-dimensional effects and device-specific features (e.g., transducer backing, housing).

5. Short duration: The 5-second heating time is representative of some HITU applications but not all (e.g., longer ablation protocols).

4.5 Implications for Regulatory Science

This work demonstrates a template for incorporating uncertainty quantification into medical device model validation. By leveraging FDA-qualified MDDT material data, the analysis provides credible uncertainty bounds that could support regulatory submissions. Key takeaways for model credibility include:

● Traceable uncertainty sources: Input uncertainties are based on publicly available FDA documentation

● Progressive analysis: Screening reduces dimensionality before expensive propagation

● Surrogate validation: GP and PCE surrogates are validated against training data

● Interpretable outputs: Prediction intervals provide actionable confidence bounds

5. Conclusions

This study developed and applied a comprehensive uncertainty quantification framework to predict focused ultrasound-induced heating in FDA-qualified tissue-mimicking material. The main conclusions are:

1. Parameter importance ranking: Attenuation coefficient (α_TMM) and speed of sound (c_TMM) are the dominant sources of uncertainty, collectively accounting for >80% of output variance. Thermal properties (k_TMM, α_diff) have secondary importance over 5-second heating, while density (ρ_TMM) is negligible.

2. Model structure: The temperature rise model is approximately additive with minimal parameter interactions, as evidenced by near-equality of first-order and total Sobol indices.

3. Prediction uncertainty: The 95% prediction interval for peak temperature rise is ±0.1 K (≈3.5% of mean), consistent with uncertainty magnitudes anticipated from FDA MDDT-specified property bounds.

4. Methodology effectiveness: The hierarchical UQ approach (MOAT screening → Sobol sensitivity → GP propagation) efficiently quantifies uncertainty with <40 model evaluations, demonstrating practical applicability for computationally intensive models.

5. Regulatory relevance: The framework provides a template for incorporating FDA MDDT data into model-based device evaluation, supporting the shift from deterministic to probabilistic performance assessment.

Future work should extend the analysis to longer heating durations, consider parameter correlations, and incorporate nonlinear acoustic propagation effects. Experimental validation with controlled TMM samples would further strengthen confidence in the uncertainty predictions.

References

1. U.S. Food and Drug Administration. (2019). MDDT Summary of Evidence and Basis of Qualification Decision for a Tissue Mimicking Material (TMM) for Preclinical Acoustic Performance Characterization of High Intensity Therapeutic Ultrasound (HITU) Devices. FDA-2017-N-3708.
2. U.S. Food and Drug Administration. (2016). Reporting of Computational Modeling Studies in Medical Device Submissions - Guidance for Industry and Food and Drug Administration Staff. FDA-2013-D-1530.
3. Morris, M. D. (1991). Factorial sampling plans for preliminary computational experiments. *Technometrics*, 33(2), 161-174.
4. Saltelli, A., et al. (2010). Variance based sensitivity analysis of model output. Design and estimator for the total sensitivity index. Computer Physics Communications, 181(2), 259-270.
5. Blatman, G., & Sudret, B. (2011). Adaptive sparse polynomial chaos expansion based on least angle regression. *Journal of Computational Physics,* 230(6), 2345-2367.
6. Rasmussen, C. E., & Williams, C. K. I. (2006). Gaussian Processes for Machine Learning. MIT Press.
7. Pennes, H. H. (1948). Analysis of tissue and arterial blood temperatures in the resting human forearm. *Journal of Applied Physiology*, 1(2), 93-122.
8. National Council on Radiation Protection and Measurements. (2002). Exposure Criteria for Medical Diagnostic Ultrasound: II. Criteria Based on All Known Mechanisms. NCRP Report No. 140.
9. Duck, F. A. (1990). Physical Properties of Tissues: A Comprehensive Reference Book. Academic Press.
10. ter Haar, G., & Coussios, C. (2007). High intensity focused ultrasound: Physical principles and devices. *International Journal of Hyperthermia*, 23(2), 89-104.
11. J. Xi,K. Barari,X. Si,M.Y.A. Jamalabadi, J. Park, M. Rein. (2022). Inspiratory Leakage Flow Fraction for Surgical Masks with Varying Gaps and Filter Materials, Physics of Fluids.
12. R. Sadeghi, M.Shadloo, M.Y.A. Jamalabadi, A. Karimipour. (2016). A three- dimensional lattice Boltzmann model for numerical investigation of bubble growth in pool boiling, *International Communications in Heat and Mass Transfer,* 79; 58- 66
13. A.Shahidian, M.Ghassemi, S.Khorasanizade, M.Y.A. Jamalabadi. et al. (2009). Flow Analysis of Non- Newtonian Blood in a Magnetohydrodynamic Pump, IEEE Transactions on Magnetics (45) 6; 2667- 2670
14. M.Y.A. Jamalabadi, J. Xi. (2022). Olfactory Drug Aerosol Delivery with Acoustic Radiation, *Biomedicine*, 10;1347
15. M.Y.A. Jamalabadi, M.Shirazi, H.Nasiri, MR. Safaei,TK. (2018). Nguyen, Modeling and analysis of biomagnetic Blood Carreau fluid flow through a stenosed artery with magnetic heat transfer; a transient study, *PLoS ONE*,13(2): e0192138
16. M.Y.A. Jamalabadi, A. Bidokhti, H. Rah, S. Vaezi, P. (2016). Hooshmand Numerical Investigation of Oxygenated and Deoxygenated Blood Flow through a Tapered Stenosed Arteries in Magnetic Field. *PLoS ONE* 11;6. (12): e0167393. 1-23
17. M.Y.Abdollahzadeh Jamalabadi, P.Hooshmand, A.Hesabi, M.K.Kwak, I.Pirzadeh. et al. (2016). Numerical Investigation of Thermal Radiation and Viscous effects on Entropy Generation in Forced Convection Blood Flow Over Axisymmetric Stretching Sheet, entropy, (18) 6; 203-218
18. S.Bita, M.Y.A. Jamalabadi, M. Mesbah. (2015). Toxicity study of silver nanoparticles synthesized using seaweed Sargassum angustifolium in common carp, Cyprinus carpio, Journal of Chemical and Pharmaceutical Research, (7) 11;91-98
19. M.Y.A. Jamalabadi, S. Dousti. (2015). Feasibility study of magnetic effects on silver nanoparticles for drug and gene

delivery in Cyprinus carpio, *Journal of Chemical and Pharmaceutical Research*, (7) 12; 206-218

20. M.Y.A. Jamalabadi. (2016). Microrobots Propulsion system design for drug delivery, *Journal of Chemical and Pharmaceutical Research*, (8) 2; 448-469
21. M.Y.A. Jamalabadi, A. Keikha. (2016). Fluid- Solid interaction modeling of Cerebrospinal fluid absorption in arachnoid villi, Journal of Chemical and Pharmaceutical Research, (8) 2; 428-442
22. A. Keikha, M.Y.A. Jamalabadi. (2016). Optimal design of magnetic field for reaction control in drug delivery applications, *Journal of Chemical and Pharmaceutical Research,* 8(5); 420-428
23. A. Keikha, M.Y.A. Jamalabadi. (2016). Numerical viscous heating effects in renal artery stenosis under peristaltic wall motions, *Journal of Chemical and Pharmaceutical Research*, 8(5); 689-706
24. S. Bita, A. Keikha, M.Y.A. Jamalabadi. (2016). Toxicity study of silver nanoparticles synthesized using aqueous and alcoholic extract of seaweed Sargassum angustifolium in Barbus sharpeyi, Journal of Chemical and Pharmaceutical Research, 8(5);707-712
25. M.Y.A. Jamalabadi. (2021). Use of Nanoparticle Enhanced Phase Change Material for Cooling of Surface Acoustic Wave Sensor, *fluids,*6, 31
26. P. Hooshmand, M.Y.A. Jamalabadi, H. K. Balotaki. (2016). MHD effects on magnetic silver nanoparticles oxidative stress and apoptosis in Cyprinus carpio, *International Journal of Pharmaceutical Research and Allied Sciences*, (5) 2; 293-304
27. M.Y.A. Jamalabadi, A. Keikha. (2016). Numerical investigation of Magneto hydrodynamics effects on natural silver nanoparticles from Sargassum angustifolium used for transporting a pharmaceutical compound in Cyprinus carpio, *Entomology and Applied Science Letters*, (3) 2;52-64
28. M.Y.A. Jamalabadi. (2016). Energy harvesting by micro-turbine in blood arteries for bio applications*, International Journal of Pharmaceutical Research and Allied Sciences*, (5) 3;52-74
29. M.Y.A. Jamalabadi, M. Shirazi, A. Kosar, M. Shadloo. (2017). Effect of injection angle, density ratio, and viscosity on droplet formation in a microfluidic t-junction, *Theoretical and Applied Mechanics Letters*, Pages 243-251
30. M.Y.A. Jamalabadi. (2026). A Molecular Key to the Filter: Podocin Phosphorylation Unveiled in a Case of Early-Stage Steroid-Resistant Nephrotic Syndrome, *Annals of Clinical and Medical Case Reports*;15 (1) 1-11
31. M.Y.A. Jamalabadi. (2025). A Conservative Numerical Framework for Modeling Nonlinear Ultrasound Propagation in Thermo-viscous Tissue Phantom, *Mathews Journal of Surgery*; 8(2) 41, 1-11.
32. M.Y.A. Jamalabadi. (2025). A Comprehensive Review of Computational Modeling in Tumor and Brain Disorder with a Focus on Ablation Therapies, *Journal of Biomedical Research Environmental Sciences*; 6(10) 19-35
33. M.Y.A. Jamalabadi. (2025). Cracking the Molecular Matrix: Next-Gen AI Reshapes Biomedicine, *World Journal of Pharmaceutical and Healthcare Research*; 2(8) 19-35
34. M.Y.A. Jamalabadi. (2025). Smart Lubrication for Joints: Carbon Nanomaterials in Biomedical Applications, *Journal of Applied Mechanics Reviews and Reports*;1(1) 1-13
35. M.Y.A. Jamalabadi. (2025). A Comprehensive Review on Deep Learning for Genomics and AI in Drug Discovery.
36. M.Y.A. Jamalabadi. Superiority of Carbon Nanocomposites on Diarthrosis Lubrication, New Energy Exploitation.
37. A. Hosseinian, M.Y.A. Jamalabadi. (2024). Numerical Investigation of Temperature Field in Hyperthermia Considering Diffusion in Interstitial Tissue, Available at SSRN 4786896.
38. M.Y.A. Jamalabadi, Electrohydrodynamic Squeeze- Film Interaction in Synovial Joints, Recent Progress in Materials 4; 1- 21
39. M.Y.A. Jamalabadi. (2022). Parameter study of the J- integral over a craze line in a root canalled tooth, *Medical Research and Innovations*, 6;1- 5
40. M.Y.A. Jamalabadi. (2026). Cerebral Aneurysm Hemodynamics: from Computational Modeling to Clinical Translation. *Archives in Neurology Neuroscience*;18(3) 10.33552/ANN.2026.18.000936